International Journal of Modern Manufacturing Technologies
ISSN 2067–3604, Vol. XIV, No. 1 / 2022
https://doi.org/10.54684/ijmmt.2022.14.1.39

INVESTIGATION ON FAILURE CONDITIONS IN DRAWING METAL POWDER-CORED RODS

Radu Ioachim Comăneci[1], Constantin Mirea[2]

[1]"Gheorghe Asachi" Technical University of Iasi-Romania, Department of Technologies and Equipments for Materials Processing, Faculty of Materials Science and Engineering, D. Mangeron 41, Iasi, 700050, Romania
[2]"Gheorghe Asachi" Technical University of Iasi-Romania, Department of Materials Engineering and Industrial Security, Faculty of Materials Science and Engineering, D. Mangeron 41, Iasi, 700050, Romania

Corresponding author: Radu Ioachim Comăneci, comaneci@tuiasi.ro

Abstract: The metal-cored wires/rods are promising and widely used welding materials for electric-arc welding. Used for specific applications metal-cored rods give the benefit of being able to have alloy compositions formulated for a certain technological purpose having high deposition rate and efficiency, high travel speed and low slag volume. During the manufacturing process by drawing through a series of dies, both sheath and powder-core deform. The initially non-compacted mixture of powder is progressively, densified and its density/porosity is redistributed as radial and longitudinal gradients over the internal volume of the rod in all stages of drawing. The higher the compactness degree of the powder-core, the higher the arc welding stability and the quality of the deposited material. The features of the drawn metal-cored rods strongly depend on the internal pressure exerted by the sheath on metal powder and vice versa. Inherent failure of the sheath will appear if a proper processing design (i.e. sequence of drawing, partial/total reduction, friction, initial coefficient of fullness, etc.) is not set. The paper aims to investigate the behavior of the sheath and metal powder as whole to prevent the failure in drawing metal-cored rods. Two drawing sequences having different process and material parameters were analyzed and the optimum scenario was chosen to keep the sheath of the rod during drawing. It was found that decreasing the reduction during first passes could preserve the rod, which can become the starting point to obtain an optimum starting point for further drawing.

Key words: Drawing, Powder-cored rods, Tensile testing.

1. INTRODUCTION

Tubular electrodes in terms of metal powder-cored wires/rods combine the best properties of solid wires/rods with flux-cored wires/rods. Because it is relatively easy to adjust alloy compositions, metal-cored rods are being found in smaller batches in new areas of application such as thermal spraying for corrosion and wear-resistant structures (Metlitskii, 2008). By changing the composition of the metal powder in the core, manufacturers can formulate different metal-cored rods to meet a variety of applications, being in high demand around the world as welding consumables in specific technologies (Crespo et al., 2008). Metal-cored consumables are composites with a tubular construction consisting of a thin metal sheath (low-carbon steel) that encloses the powder core which is made of elemental and alloyed metal powders with or without nonmetallic compounds for slag forming, arc stability, and deoxidation (Sun et al., 2007). These consumables are available as metal-cored wires and strips, coated tubular electrodes, and metal-cored rods having a compositional flexibility given by the core composition and filling factor. Inherent chemical and granular heterogeneity of the core due to the mixing manufacturing process affect the arc welding stability (Shalimov and Tabatchikov, 2010). Different produc-tion methods are available for tubular wires (Chigarev and Belik, 2012). Metal-powder can fill an open or a closed-volume shape. In the first case, a U-shaped thin strip is filled with powder, rolled into a circular section followed by reduction to the final diameter by rolling. In the second case, a longitudinally welded tube is filled with powder, sealed and reduced to final diameter by drawing. The round tube passes through several drawing dies that further reduce the diameter and at the same time compress the core ingredients. The compacting of the core has a key role in welding process because the melting mode and metal transfer into the weld pool are very sensitive to the level of core compaction. In melting process, the sheath and core do not melt as a whole, only a fraction of overall thickness of the core melts simultaneous with the metal sheath (Starling and Modenesi, 2007). The degree of inhomogeneity of weld metal increases with the decreasing of the filling ratio. The higher the compactness degree of the powder-core, the higher the arc welding stability and the quality of the deposited material (Chigarev et al., 2006). During gradual reduction of initial tube diameter, compaction of the core occurs, preventing its free axial movement. In the

first stage of the reduction process, the interaction sheath-core does not affect the wall thickness, but as the powder becomes compacted, the tube wall is thinned. Using a high degree of reduction before powder being compacted can lead to longitudinal moving of the powder, resulting in a varying filling ratio and wall thickness (Chigarev et al., 2012). As in the tube sinking, inner diameter (i.e. thickness of the tube wall) cannot be controlled during drawing. So, the wall thickness will not be the same along the full length of the rod. There is a direct relationship between thickness of the tube wall and the densification of the powder-core. After the powder achieves a certain compaction degree, the wall thickness of the tubular rod depends only on its final diameter and the amount of powder from initial blank (Chigarev et al., 2012). The impact of shell thickness on the power parameters and powder core density during powder wire flattening was studied too (Gribkov and Perig, 2016). Thinning of the tube walls gives higher drawing stresses. When the current axial stress exceeds the strength of the sheath, the failure occurs.

The present study aims to give a sustainable analyzing tool of the metal powder-cored rods manufacturing process so that drawing failure by sheath damage can be avoided. Results show that the global admissible reduction depends not only on the sheath dimensions but also on the level of powder-core compaction that actually gives the stress state as interaction between metallic sheath and powder core on one hand and metallic sheath and the die on the other hand. The wall thickness along the length of the rod after two and four drawing passes respectively - as direct effect of densification of the powder core - was studied. Substantial transverse nonuniformity in the hardness distribution across the sheath caused by nonuniform radial strain as effect of heterogeneous compaction of the powder core was found. It has been shown that a drawing design consisting in smaller progressive reductions instead of larger and fewer reductions is the optimum drawing design that could avoid the damage of the sheath.

2. DRAWING PROCESS VARIABLES

Figure 1 shows the principle of metal powder-cored rods drawing, emphasizing the variables that depict geometry of the rod during *i* pass.

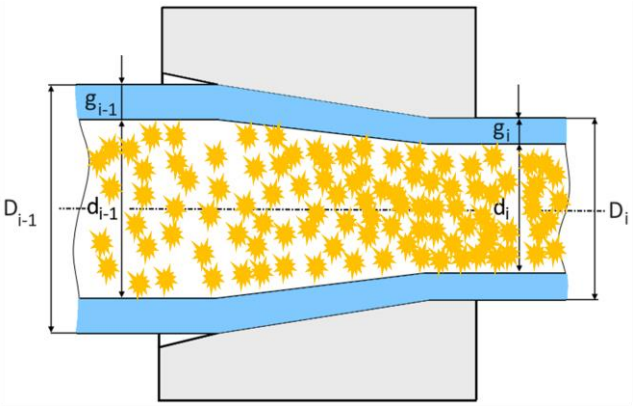

Fig. 1. Schematic principle and geometry of metal powder-cored rods drawing

The process variables related to geometry are partial and total relative elongation for pass *i* (λ_i; $\lambda_{tot\,i}$) and cross-sectional area reduction (r_i; $r_{tot\,i}$).

$$\lambda_i = \frac{L_i}{L_{i-1}}; \quad \lambda_{toti} = \frac{L_i}{L_o} \tag{1}$$

where L_o, L_{i-1} and L_i are the initial length and length after *i-1* and *i* pass, respectively.

$$r_i = \frac{A_{i-1} - A_i}{A_{i-1}} = 1 - \frac{A_i}{A_{i-1}} = 1 - \frac{1}{\lambda_i}, \text{where } A_{i-1} = \pi\left[\left(\frac{D_{i-1}}{2}\right)^2 - \left(\frac{d_{i-1}}{2}\right)^2\right]; \quad A_i = \pi\left[\left(\frac{D_i}{2}\right)^2 - \left(\frac{d_i}{2}\right)^2\right] \tag{2}$$

$$r_{toti} = \frac{A_o - A_i}{A_o} = 1 - \frac{A_i}{A_{i-1}} = 1 - \frac{1}{\lambda_{toti}}, \text{where } A_o = \pi\left[\left(\frac{D_o}{2}\right)^2 - \left(\frac{d_o}{2}\right)^2\right] \tag{3}$$

Taking into account that $g_{i,\,i-1} << D_{i,\,i-1}$, $d_{i,i-1}$, the relationships between diameters and thickness are:

$$\frac{D_{i-1}}{2} = \frac{d_{i-1}}{2} + g_{i-1} \Rightarrow \left(\frac{D_{i-1}}{2}\right)^2 - \left(\frac{d_{i-1}}{2}\right)^2 = d_{i-1}g_{i-1} \text{ and } \frac{D_i}{2} = \frac{d_i}{2} + g_i \Rightarrow \left(\frac{D_i}{2}\right)^2 - \left(\frac{d_i}{2}\right)^2 = d_i g_i \tag{4}$$

so, the partial and total reduction of the cross-section r_i and $r_{tot\,i}$ from Eq. (2) and (3) can be written as:

$$r_i = 1 - \frac{d_i g_i}{d_{i-1} g_{i-1}}; \; r_{toti} = 1 - \frac{d_i g_i}{d_o g_o} \tag{5}$$

Features of metal-cored rods are also related to the coefficient of fullness defined as powder-core mass (m_p) to the total mass of the powder and tube ($m_p + m_t$):

$$k_u = m_p/(m_p + m_t)\ (\%) \tag{6}$$

3. EXPERIMENTAL

A batch of samples consisting of tubes made from low carbon steel 1.0338 - EN 10130 (≤ 0.08% C; ≤ 0.4% Mn) with initial outer diameters of 6 mm and thickness of 0.76 mm, having elongated tapered ends and a total length of 500 mm each was prepared. To emphasize the behavior of the powder-cored rods during drawing, the tubes were divided into 7 numbered segments having 50 mm lengths each (numbering corresponds to the drawing sequence, Figure 2). To avoid adverse events during filling process as specific gravity separation and segregation, iron powder was used. The gravimetric size distribution was determined according to ISO 4497:2014 standard. The compaction of the powder into the tubes was performed by using vibration, beginning with the segment no.1. To get the coefficient of fullness, the mass of the powder and then of the sealed tube were measured by using a precision balance. Two different coefficients of fulness were confirmed: k_{u1} = 39.25% and k_{u2} = 43.36%.

Drawing was performed by using a hydraulic unit having a maximum load of 100 kN and a stroke of 750 mm (Figure 2), with a drawing rate of 17...24 mm/s (maximum value corresponds to minimum outer diameter).

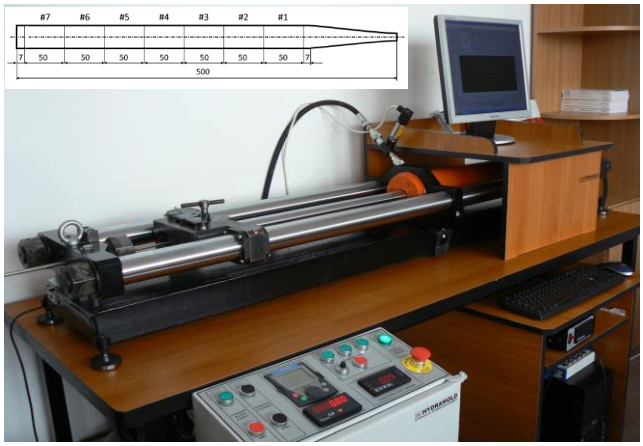

Fig. 2. Experimental drawing machine

Two different pass schedules were applied till the same final outer diameter: **A** - D_o = 6 mm → 5 mm → 4.25 mm; **B** - D_o = 6 mm → 5.5 mm → 5.0 mm → 4.5 mm → 4.25 mm.

Because of the powder-sheath interaction, a radial and longitudinal densification gradient is inherent, resulting in different thinning of the wall of the tube, i.e. non-uniform strain. This is highlighted by radial and circumferential microhardness measurements. Five equally spaced measurements across the thickness of the sheath in four orthogonal directions were performed with a Vickers indenter (CV with different pass schedule, tensile tests on the final rods were conducted at room temperature using a universal computer-controlled testing machine (Instron 3382). Tests were performed with a constant strain rate of 6.7×10^{-3} s^{-1} (that corresponds to an initial crosshead speed of 1 mm/min) applied throughout the entire test according to ISO 6892-1: 2016 recommendations in order to determine the ultimate tensile strength and elongation at fracture.

4. RESULTS AND DISCUSSIONS

Table 1 shows the drawing results in terms of relative elongation for the two coefficients of fulness k_{u1} and k_{u2}.

Obviously, the relative elongation differs both in relation to the segments and tubes on total length, being the result of the presence of the core with varying degrees of fullness.It becomes clear that the greater total elongation corresponds to the rod having the core with the highest degree of fullness. The presence of the core gives the elongation of the rod by decreasing the thickness of the wall: the more the core is compressed, the greater the elongation. The overall elongation of the segments is also differentiated: while in the empty drawing the segments extend relatively uniform, the presence of the core determines a different tendency of the elongation, as follows:

- at the minimum initial fullness coefficient (k_{u1} = 39.25%) the overall elongations of the segments decrease continuously starting from segment no.1 and this could be related to the higher compaction of the powder in the first segments due to additional gravitational effect;
- at maximum initial fullness coefficient (k_{u2} = 43.36%) the maximum segment elongation occurs at the middle of the rod (segment no. 4), which may be an indicator of the core heterogeneity along the rod: the powder is progressively compacted by its longitudinal movement inside the rod, forcing the progressive thinning of wall.

Linear mass density (mass per unit length) measurements cannot provide a direct relation linking the different elongations of the segments with the possible non-uniformity of the core, as long as there is no clear confirmation of variation in wall thickness at a certain time. To the same extent, precise determination of the fullness coefficient after a drawing pass can only be achieved by removing the core, which cannot be obtained without damaging the rod. The only solution remains the measurement of the wall thickness either by a non-destructive method (e.g. ultrasounds), or by transversely cutting the segments and performing the measurements by microscopy (Figure 3).

Table 1. Relative ($\lambda_1 ... \lambda_7$) and total ($\lambda_{tot\,i}$) elongations per segment and tube respectively for A_{ij} and B_{ij} pass for the two different coefficients of fullness (i signifies the cardinal of k_u; $i = 0$ means empty drawing; j signifies the current pass)

Code	Pass		λ_i/# segment									Coef. of fullness
	D_{i-1} (mm)	D_i (mm)	1 λ_1	2 λ_2	3 λ_3	4 λ_4	5 λ_5	6 λ_6	7 λ_7	$\lambda_{tot\,i}$	r_i	k_u (%)
A_{01}	6.00	5.00	1.22	1.24	1.22	1.24	1.24	1.22	1.22	1.24	0.19	
A_{02}	5.00	4.25	1.20	1.21	1.21	1.21	1.21	1.21	1.21	1.21	0.17	–
A_0	**6.00**	**4.25**	**1.46**	**1.50**	**1.48**	**1.50**	**1.50**	**1.48**	**1.48**	**1.49**	**0.33**	
A_{11}	6.00	5.00	1.31	1.28	1.29	1.28	1.27	1.26	1.28	1.27	0.21	**39.25**
A_{12}	5.00	4.25	1.41	1.41	1.39	1.36	1.34	1.34	1.30	1.37	0.27	✓
A_1	**6.00**	**4.25**	**1.85**	**1.80**	**1.79**	**1.74**	**1.70**	**1.68**	**1.66**	**1.74**	**0.42**	
A_{21}	6.00	5.00	1.28	1.28	1.32	1.33	1.32	1.33	1.31	1.31	0.24	**43.36**
A_{22}	5.00	4.25	1.34	1.31	1.56		✗			1.40	0.29	✗
A_2	**6.00**	**4.25**	**1.83**	**1.83**	**2.18**					**1.94**	**0.49**	
B_{11}	6.00	5.50	1.11	1.12	1.11	1.10	1.10	1.09	1.10	1.10	0.09	
B_{12}	5.50	5.00	1.15	1.17	1.17	1.16	1.18	1.19	1.20	1.18	0.15	**39.25**
B_{13}	5.00	4.50	1.09	1.08	1.09	1.09	1.09	1.09	1.09	1.07	0.06	✓
B_{14}	4.50	4.25	1.29	1.28	1.27	1.28	1.29	1.29	1.30	1.31	0.24	
B_1	**6.00**	**4.25**	**1.81**	**1.81**	**1.81**	**1.79**	**1.83**	**1.83**	**1.85**	**1.81**	**0.45**	
B_{21}	6.00	5.50	1.11	1.12	1.12	1.12	1.12	1.13	1.13	1.12	0.11	
B_{22}	5.50	5.00	1.22	1.20	1.16	1.23	1.23	1.16	1.17	1.19	0.16	**43.36**
B_{23}	5.00	4.50	1.08	1.11	1.09	1.09	1.08	1.11	1.11	1.10	0.09	✓
B_{24}	4.50	4.25	1.30	1.27	1.29	1.28	1.28	1.30	1.28	1.29	0.22	
B_2	**6.00**	**4.25**	**1.90**	**1.90**	**1.84**	**1.94**	**1.90**	**1.89**	**1.87**	**1.89**	**0.47**	

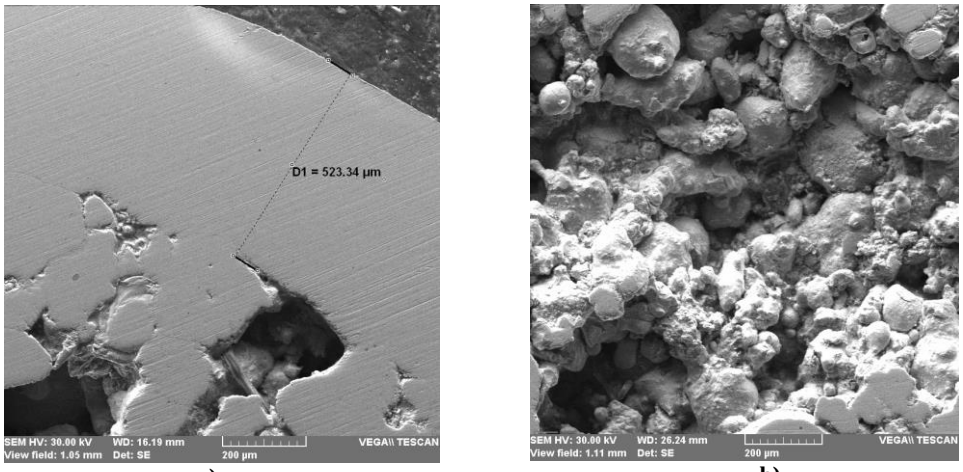

a) **b)**

Fig. 3. SEM images of the interior of the powder-cored rod near the wall (a) and in the middle of the core (b)

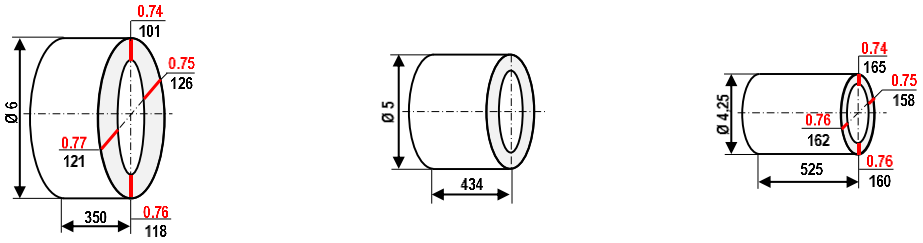

a) A_0 – empty drawing; 6 → 5 → 4.25 mm

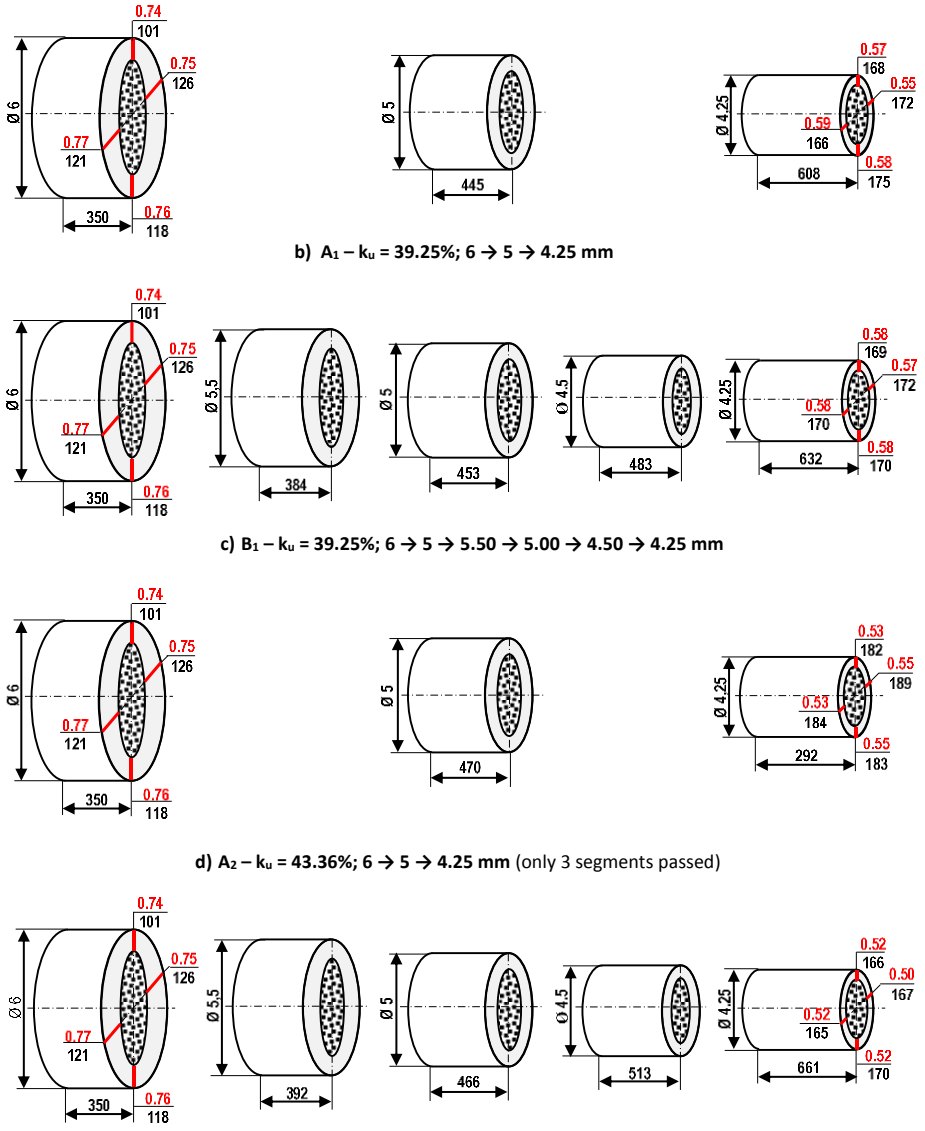

Fig. 4. Schematic representation of powder-cored rods for pass schedules A and B showing initial and final values of thickness (in red) and cross-sectional microhardness: a) A_0; b) A_1; c) B_1; d) A_2; e) B_2

As can be seen from the above figure due to intense inner pressure, powder particles penetrate the wall similar to welded joint, making difficult the thickness evaluation. At the same time, these welded joints mean a plastic flow of the sheath leading to the wall thinning. Figure 4 shows the evolution of the length, thickness and microhardness in cross sectional of the rods after the two drawing pass scenarios A and B corresponding to the two coefficients of fullness. For empty drawing (Figure 4(a)), as it was expected, no change in thickness was found, due to missing core.

As can be seen from Table 1, for the coefficients of lightly from 0.42 (A_1) to 0.45 (B_1) in accordance with the total relative elongation ($\lambda_{tot\ i}$). Increasing the length doesn't lead to a significant thinning of the wall (Figure 4(a), (b)). It is true that those values are average values and cannot describe accurately the longitudinal non-uniformity of the wall thickness. Increasing the coefficient of fullness leads to the failure of the sheath during the second pass of the A_2 scenario when drawing is under way: only the first three segments passed through the die (Figure 5(d)).During drawing, the total reduction in four passes (B_2) leads to a smaller total reduction of 0.47 so the sheath was preserved.

Moreover, a noticeable work hardening revealed by higher hardness takes place. In contrast to the previous case, the fragmentation of the reduction in four passes (B_2) leads to a smaller total reduction of 0.47 so the sheath was preserved. That because of less intense work hardening. This can be confirmed by tensile testing results (Figure 5).

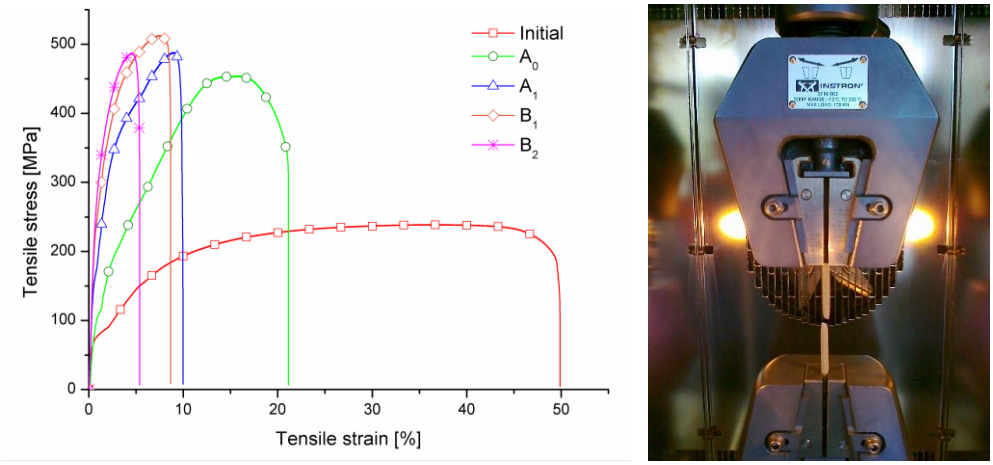

Fig. 5. Tensile testing results for the drawn tubes

Each tensile test was performed on the segment no. 4 being positioned at the middle of the rod. Therefore, the A_2-test is missing because the failure of the sheath occurred exactly across the segment no. 4 when drawing was actually unfinished.

From Figure 5 one can see that B_1 and B_2 scenarios with four passes instead of two passes have similar evolutions. Moreover, transposing graphs into stress vs. strain coordinates, the mathematical expression of the two corresponding flow curves are $\sigma = 1391 \cdot \varepsilon^{0.338}$ (B_1) and $\sigma = 1516 \cdot \varepsilon^{0.339}$ (B_2) which have similar coefficients of work hardening.

The tensile stress vs. tensile strain graph of the initial tube gives an elongation at fracture of 50%, very close to the reduction of 49% corresponding to A_2 scenario when failure of the sheath was recorded.

5. CONCLUSIONS

Two different drawing schedules (**A**: 6 → 5 → 4.25 mm and **B:** 6 → 5.5 → 5.0 → 4.5 → 4.25 mm) with two different coefficients of fullness were experimentally performed. For the minimum coefficient of fullness, no matter the chosen pass schedule, the fragmentation of the strain has a little impact due to a limited influence of the core, especially during the first pass. Increasing the coefficient of fullness leads to the failure of the sheath during the last pass of the A schedule because of the highest reduction reached during the first pass. Further fragmentation of deformation avoids too much reduction during the first pass, decreasing the negative effect of the core on the sheath due to the non-uniform compaction of the core. In both scenarios, fragmentation of the total deformation leads to a higher reduction, preserving the sheath.

6. REFERENCES

1.Chigarev, V. V., Belik, A. G., Sergienko, Yu. V., (2006), *Design experimental assessment of the features of electrode melting and transfer process*, Paton Weld. J. **8**, 7-10.

2.Chigarev, V. V., Gavrish, P. A., Gribkov, E. P., (2012), *Investigation of the process of drawing flux-cored wire for welding copper to steel*, Weld. Int. **26**(9), 718-722.

3.Chigarev, V.V. and Belik, A.G., (2012), *Flux-cored strips for surfacing*, Weld. Int. **26**(12), 975-979.

4.Chigarev, V. V., Belik, Gribkov, E. P., Gavrish, P. A., (2015), *A mathematical model of the process of rolling flux-cored tapes*, Welding International Weld. Int. **29**(1), 70-74.

5.Crespo, A. C., Scotti, A., Pérez, M. R., (2008), *Operational behavior assesment of coated tubular electrodes for SMAW hardfacing*, J. Mater. Proc. Tech. **199**(1-3), 265-273.

6.Gribkov, E.P., and Perig, A.V., (2016), *Research of energy-power parameters during powder wire flattening*, Int. J. of Adv. Manuf. Tech. **85** (9-12), 2887-2900.

7.Metlitskii V. A., (2008), *Flux-cored wires for arc welding and surfacing of cast iron*, Weld. Int. **22**(11), 796–800.

8.Shalimov, M. P. and Tabatchikov, P. A., (2010), *Methods of Assessing Homogeneity of Wire Core Flux*, The Sixth International Conference on Mathematical Modeling and Computer Simulation of Materials Technologies MMT-2010, September 23-27, Ariel, 47-54.

9.Starling, C. M. D., and Modenesi, P. J., (2007), *Metal transfer evaluation of tubular wires*, Weld. Int. **21**(6), 412-420.

10.Sun, J. S., Jiao, E. L., Wang, H. M., (2013), *The Design and Application of Flux-Cored Strip for Surfacing*, Adv. Mater. Res. 753-755, 363-366.

Received: January 11, 2021 / Accepted: June 15, 2022 / Paper available online: June 20, 2022